



OPEN Pipeline for development of acylated peptide based CGRP receptor antagonist with extended half-life for migraine treatment

Jens Bjelke Kristensen^{1,2}✉, Lisbeth Elster¹, Morten Lundh¹, Borja Ballarín-González^{1,3}, Flora Alexopoulou^{1,3}, Martin Kræmer¹, Ditte Marie Jensen¹, Ulrike Leurs¹, Jens Christian Nielsen¹, Henrik H. Hansen¹, Kristian A. Haanes^{2,4,5,6} & Matilda Degn^{1,6}✉

Migraine is a debilitating headache disorder. The disease has neurovascular origin and migraine attacks can be elicited by vasodilative neuropeptides such as alpha calcitonin gene-related peptide (α CGRP). Antagonizing CGRP actions in migraine patients has proven clinically efficient. Here, we present a pipeline for development of a peptide-based hCGRP receptor antagonist with increased half-life capable of antagonising the vasodilatory effect of hCGRP. A series of hCGRP8-37 analogues carrying a C18-or C20-diacid lipidation was screened for their antagonism against the hCGRP receptor. hCGRP8-37 analogues with a C20-diacid were 2-6 fold more potent than analogues conjugated with a C18-diacid. Half-life of hCGRP8-37 analogues carrying a C20-diacid was estimated in mice in a pilot study ($n=1-2$). Half-lives ranged from 7.3 to 13.7 h. An hCGRP8-37 analogue conjugated with a C20 diacid at position 25 was subjected to an amino acid substitution scan to identify mutations that could further enhance hCGRP receptor antagonism. Substituting alanine with serine at position 36 resulted in a ~4 fold gain of potency. Vasodilative actions of hCGRP were successfully antagonized by hCGRP8-37 analogues carrying a C20 diacid at position 25. Our findings demonstrate that lipidation can improve hCGRP8-37 pharmacokinetics while maintaining hCGRP antagonism, thus demonstrating potential for a peptide-based migraine treatment strategy.

Calcitonin gene-related peptide (CGRP) is a prominent target in migraine treatment. CGRP is a 37-amino acid neuropeptide with two isoforms, α CGRP and β CGRP, which are expressed by two distinct genes¹. The α -isoform is primarily located in the central and peripheral nervous system, and the β -isoform primarily acts on the enteric nervous system^{2,3}. The α -isoform is believed to be the main inducer of migraine⁴. α CGRP regulates a variety of physiological processes by targeting heterodimeric G-protein coupled receptors to promote intracellular generation of cAMP via the adenylate cyclase pathway⁵.

The exact role of α CGRP in migraine is only partly understood, since α CGRP is widely distributed in the body and regulates numerous functions. These functions range from regulation of energy homeostasis⁶, vasodilation⁷ and sensitization of nociceptive nerve fibres⁸. α CGRP is believed to mediate migraine through dural vasodilation and pain sensitization of A δ -fibres via cAMP-dependent pathways⁹⁻¹¹. These mechanisms are considered to be mediated through the calcitonin receptor-like receptor (CLR) and the receptor activity-modifying protein 1 (RAMP1). This CLR:RAMP1 receptor complex is commonly referred to as the CGRP receptor (CGRP-R)¹².

Several therapeutics that block the action of α CGRP have been approved for treatment of migraine. Therapeutics that block the CGRP-R include the small molecule drugs, gepants¹³, and the monoclonal antibody, erenumab^{14,15}. The monoclonal antibody, fremanezumab, targets α CGRP and prevents its binding to the receptor¹⁶. The serotonin receptor agonists, triptans, inhibit α CGRP release from nerve terminals^{17,18}.

Peptide-based α CGRP antagonists have been considered as potential migraine therapeutics¹⁹⁻²³. Peptide therapeutics are attractive drug classes due to low immunogenicity, high target specificity, good safety profile,

¹Gubra ApS, Hørsholm Kongevej 11B, DK-2970 Hørsholm, Denmark. ²Sensory Biology Unit, Translational Research Centre, Copenhagen University Hospital - Rigshospitalet, Glostrup, Denmark. ³Novo Nordisk, Måløv, Denmark. ⁴Department of Biology, Section of Cell Biology and Physiology, University of Copenhagen, Copenhagen, Denmark. ⁵Department of Neurology, Danish Headache Center, Copenhagen University Hospital - Rigshospitalet, Copenhagen, Denmark. ⁶Kristian A. Haanes and Matilda Degn contributed equally to this work. ✉email: jbj@gubra.dk; mvi@gubra.dk

and low production costs²⁴. The first identified peptide-based CGRP-R antagonist was the N-terminal truncated α CGRP analogue, α CGRP8-37, which lacks the receptor activating domain²⁵. α CGRP8-37 binds to the CGRP-R and blocks binding by CGRP, thus acting as a competitive antagonist. Due to short half-life, α CGRP8-37 is not suited as clinical drug candidate^{19,25}. In attempts to increase half-life of α CGRP8-37, pharmacokinetic properties of haCGRP8-37 have been improved by various peptide modifications such as PEGylation²⁰ and cyclization²¹. However, to date no α CGRP8-37 based therapeutics have been profiled in clinical trials.

Fatty acid lipidation has proven effective for increasing albumin binding and thereby improving the circulating half-life of peptide therapeutics^{26–28}. Through attachment of lipid moieties, the acylated peptide can bind to serum albumin, which enables protection against renal excretion and enzymatic degradation^{29,30}. In addition, adding a spacer such as γ -glutamic acid (γ Glu) as anchor between the lipid and the peptide is reported to promote hydrophilicity of the peptide therapeutic and result in improved *in vivo* efficacy^{27,31,32}.

Jamaluddin et al. (2022) provided proof of concept of peptide lipidation in migraine therapeutic by demonstrating that a series of palmitoylated haCGRP8-37 analogues maintained antagonism against the hCGRP-R and antagonized α CGRP *in vivo*²². However, pharmacokinetics of lipidated analogues of haCGRP8-37 pharmacokinetics has not been explored.

In this study, we applied the peptide drug discovery platform, streaMLine, to study hCGRP-R antagonism of a comprehensive series of lipidated haCGRP8-37 analogues. StreaMLine is a drug discovery platform that facilitates peptide-based drug discovery by enabling synthesis and characterization of several thousand crude peptide³³. In this present study, the streaMLine platform was used to synthesize and characterize a series of lipidated haCGRP8-37 analogues with extended half-life. In addition, a comprehensive amino acid mutational scan was performed on a selected lipidated haCGRP8-37 analogue to identify amino acid substitutions which further enhance potency against the hCGRP-R.

Materials and methods

Animals

Work involving use of animals compiled with the ARRIVE guidelines. Mice used for the pharmacokinetic study were housed in the AAALAC accredited animal facility at Gubra, Denmark. The Experiment are licensed by the Danish Animal Experimentation Inspectorate, license no. 2023-15-0201-01508. Six-week old male NMRI mice were obtained from Janvier (France). One week prior to study start the animals were single housed in Cage Type I L (Opend, Denmark) a controlled environment at a temperature of 21 ± 2 °C, relative humidity $50 \pm 10\%$, with a 12:12-h light–dark cycle in cages with bedding material, and shelters and free access to regular chow (Altromin 1324, Brogaard, Denmark) and water. Animals were checked once daily for signs of abnormal behaviour, wounds or clinical signs of pain or disease. For pharmacokinetics studies involving analysis of compound exposure in mice, 50 μ l tail blood was drawn from each mouse at 5 min, 1 h, and 6 h post dosage. The 24 h terminal sample was taken from the heart under anesthesia with isoflurane. Blood sampling adhered to the bioethical guidelines of Gubra under license 2017-15-0201-01378 issued by the Danish Animal Experimentation Council. Animal study designs, and associated care were approved by the Gubra Institutional Animal Care and Use Committee (IACUC), ensuring compliance with all regulatory standards.

The rats used for the myography experiments were approved by the Danish Animal Experimentation Inspectorate, license no. 2020-15-0201-00751. The animal procedures adhered to the European Community Council Directive on "The protection of Animals Used for Scientific purposes" (2010/63/EU) and were approved by the Danish Animal Experimentation Inspectorate. Male Sprague–Dawley rats (NTac:SD, approximately 400 g) from Taconic (Ejby, Denmark) were group housed in Eurostandard cages (Type VI with 123-Lid) at the animal facility at Rigshospitalet Glostrup, Denmark with free access to bedding material, shelters and free access regular chow and water in a controlled environment 12/12-h dark–light cycle, constant temperature (22 ± 2 °C), and humidity ($55 \pm 10\%$). For each experiment, the rats were sedated with O₂/CO₂ (30/70%) and euthanized by decapitation.

Peptide synthesis

Peptides were synthesized by standard 9-fluorenylmethoxycarbonyl (Fmoc) solid phase peptide synthesis (SPPS) on a SyroII Parallel Peptide Synthesizer (MultiSynTech GmbH, Witten, Germany) in either 0.008, 0.1, or 0.2 mmol scale using TentaGel S RAM resins (0.22 mmol/g) as solid support (Rapp Polymere GmbH). Standard couplings were performed by adding the 5 equivalents amino acid solution [0.5 M in DMF (N-methyl-2-pyrrolidone (NMP) for Phe) containing 0.5 M ethyl 2-cyano-2-(hydroxyimino)acetate (OxymaPure)] followed by addition of 1.0 M solution of N,N'-diisopropylcarbodiimide (DIC) (5 equivalents) in DMF. Resins were heated to 75 °C for 15 min (50 degrees Celsius for His). C18 diacid (C18DA) and C20 diacid (C20DA) lipids (AstaTech Inc., Bristol, PA, USA) were coupled as the mono-tert butyl protected diacids, while ethylene glycol spacers (OEG) and γ Glu were coupled as Fmoc-OEG-OH or Fmoc-OEG-OEG-OH and Fmoc-L-Glu-OtBu (Iris Biotech GmbH) using the standard coupling conditions described above. Lipidations were performed with N-terminal boc-protection and Fmoc-Lys(Mtt)-OH at positions for lipidations. Subsequent Mtt-deprotection with 75% hexafluoroisopropanol (HFIP) in dichloromethane (DCM) with 5% triisopropylsilane (TIPS). Cleavages were performed using trifluoroacetic acid (TFA), MilliQ water, TIPS, and 3,6-dioxo-1,8-octanedithiol (DOTD) in a ratio 93:2:2.5:2.5 (v/v) at 40 degrees Celsius for 45 min. Precipitation in cold diethyl ether and dissolution in MilliQ water/acetonitrile 1:1 (v/v) was done prior to lyophilization. Peptide identities and purities were determined by LC–MS on an ACQUITY UPLC H-Class Series with an SQD2 single quadrupole mass detector (Waters, Tåstrup, Denmark) equipped with an ACQUITY Premier Peptide CSH C18 Column (1.7 μ m, 2.1 \times 100 mm, 130Å, Waters). Peptides were analyzed with a flow rate of 0.3 mL/min using a linear gradient from 10–80% eluent B over 12 min. Peptide quantities were determined using a Vanquish UPLC system with a Charged Aerosol Detector (ThermoFisher Scientific, Waltham, MA, USA) equipped with a Luna Omega C18

column (1.6 μm , 50 \times 2.1 mm, 100 \AA . Phenomenex, Torrance, CA, USA). Peptides were analyzed with a flow rate of 0.5 mL/min using a linear gradient from 0–80% eluent B over 7 min. Peptide LC–MS chromatograms assisted in the integration of the CAD chromatograms to generate the purity-corrected peptide quantification used for peptide aliquotation. Peptide purifications were carried out by semi-preparative HPLC on an LC Prep 150 system (Waters) equipped with a Reprosil Gold C18 column (5 μm , 30 \times 250 mm, 200 \AA . Dr. Maisch, Ammerbuch, Germany) using a flow rate of 40 mL/min. Eluents for all LC systems: A: 0.1% TFA in MilliQ water. B: 0.1% TFA in Acetonitrile.

In vitro measurements of cAMP

Time resolved fluorescence was applied to measure cAMP. The assay technology has thoroughly been described in the CisBio HTRF cAMP assay Kit manual (# 62AM4PEC).

CHO-K1 cells stably expressing the human calcitonin gene-related peptide receptor (PerkinElmer #ES-420-C stable monoclonal hCGRP-R cell line) were thawed from frozen cell stocks immediately before assays.

384-Well (Corning, #4513) assay formats were applied with a total assay volume of 20 μl . The applied assay buffer was DPBS (Sigma, #D8537) containing 0.5 mM IBMX (Sigma, # I5879) and 0.05% casein (Sigma, # C4765-10ml). 2,000 cells were used per well. In all assays, antagonists were applied to the cells, followed by immediate addition of the agonist. Cells were then incubated for 30 min at room temperature.

After the addition of HTRF[®] detection reagents and incubation for 1 h on a plate shaker (2400 rpm), signals at 620 and 665 nm (raw counts: ratio of 665/620 nm) were detected at a ClarioStar plate reader (BMG Labtech, Ortenberg, Germany). When analysing antagonist potency, E_{min} refers to cAMP levels generated from 24 pM haCGRP, which corresponds to haCGRP_{EC90} (0% inhibition).

E_{max} refers to cellular cAMP in the absence of agonist stimulation (100% inhibition). Potency of antagonists is described as IC50, which refers to the antagonist concentration that induces 50% inhibition of the response from haCGRP.

When analysing potency of haCGRP in the presence of various concentrations of antagonist, E_{min} refers to cAMP levels of CHO-K1 cells without haCGRP stimulation (0% activation). E_{max} refers to cAMP levels at 1 nM haCGRP (100% activation). An independent experiment is denoted as $n = 1$. The number of experimental replicates is presented in figure legends.

The CHO-K1 cell line endogenously expresses other members of the calcitonin family of receptors³⁴. Therefore, RNA sequencing was performed on the purchased cell line prior to initiation of this study. This analysis confirmed the overexpression of CALCRL and RAMP1. In addition, potency of hAmylin and hCGRP was compared. A consistent 750-fold lower EC50 for hCGRP compared to hAmylin was observed (1.6 pM vs 1.2 nM).

Mass spectrometry for compound exposure analysis

For determination of pharmacokinetic profile, 700 nmol/kg of each selected lipidated peptide were administered intravenously (IV). For estimation of half-lives, experimental units are denoted as $n = 1$ and correspond to a single mouse IV dosed with compound. Blood was sampled at $t = 5$ min, 1 h, 6 h and 24 h after IV dosing in K2-EDTA tubes followed by centrifugation at 3000 \times g for 10 min. The plasma supernatant was stored at -70 °C until analysis.

Plasma proteins were removed by addition of 1:4 plasma:MeOH (v/v) followed by centrifugation at 2670 \times g for 40 min at 4 °C. The supernatant was analyzed by LC-MSMS using an Exploris120 mass spectrometer coupled to a Vanquish Tandem UPLC (both Thermo Fisher) equipped with an Acquity BEH C18 column (1.7 μm , 2.1 \times 50 mm, 130A, Waters). Peptides were eluted using a linear gradient starting at 5% over 7.5 min to 70% buffer B at a flow rate of 0.4 mL/min at 40 °C (buffer B = 100% acetonitrile with 0.1% formic acid; buffer A = 100% water with 0.1% formic acid). Data were acquired in data-dependent acquisition mode at an MS1 resolution of 60,000, and an MS2 resolution of 30,000 in positive mode (Top4). Peptides were fragmented with a normalized collision energy of 25%. Peptides were quantified based on the extracted ion chromatogram (EIC) of their highest isotopic peak. For each compound, a calibration curve prepared and analysed along with the plasma samples.

Wire myography

The mesenteric arcade was isolated and placed in cold, oxygenated physiological solution with the following composition: 119 mM NaCl, 4.7 mM KCl, 2.5 mM CaCl₂, 25 mM NaHCO₃, 1.17 mM MgSO₄, 1.18 mM KH₂PO₄, 5.5 mM glucose, 0.03 mM (Kreb's buffer). Subsequently, 2nd order mesenteric branches were isolated from the mesenteric arteries under a microscope. Each arterial segment was cut into a 1.0–1.6 mm segments and mounted on two 40 μm wires in an organ bath of a small vessel wire myograph (DanishMyo Technology A/S, Aarhus, Denmark).

After mounting in myographs, arteries were allowed to equilibrate for 30 min in Kreb's buffer. The buffer was aerated with 5% CO₂ / 95% O₂ to maintain a stable pH at 7.4. After equilibration, vessels were stretched to their optimal lumen diameter $L1 = 0.9 \times L100$, where L100 is an estimate of the diameter of the vessel under a passive transmural pressure of 100 mmHg (13.3 kPa). Vessels were then allowed to equilibrate for approximately 30 min before being exposed twice to a bicarbonate buffer containing 60 mM K⁺ to induce contraction of arteries, thus confirming their viability. Arteries that exhibited a 2 mN increase in force were selected for the experiments. Measurements of isometric tension of the arteries were recorded with a Power Lab unit (ADInstruments).

An experimental unit corresponds to a single rat and is denoted as $n = 1$. For each experiment, segments were isolated from a single artery and attached in myographs. One segment served as an haCGRP-dose–response control while other segments were incubated with a fixed concentration of antagonist. To minimize potential variation in responses to haCGRP between arteries, control segments were isolated from the same artery as segments incubated with antagonists in all experiments. Concentration–response curves to haCGRP were

generated for each artery following a stable precontraction with 200 nM U46619. Each segment was exposed to progressively increasing concentrations of hαCGRP until the tension generated from the arteries returned to the resting state. The arterial tension generated by 200 nM U46619 was denoted as E_{\min} (0% relaxation). The tension generated during the resting state was denoted as E_{\max} (100% relaxation).

Data analysis

All statistical analyses were conducted using GraphPad Prism Version 9.4.1 (GraphPad Software). Concentration–response curves to hαCGRP were analysed by 4-parameter non-linear regression analysis with GraphPad Prism 9.4.1. Data from independent experiments were normalized to E_{\max} and E_{\min} and pooled into single dose response curves.

For Schild analysis, $\log [DR-1]$ was plotted against $\log [Antagonist (M)]$ and analysed with linear regression analysis in GraphPad Prism 9.4.1. DR is the ratio between agonist EC50 in the presence and absence of antagonist. Plotting $\log [DR-1]$ against $\log [Antagonist]$ enables determination pA_2 through estimation of the x-intercept. pA_2 is the log concentration of antagonist that induces a two-fold shift in agonist EC50. If the Schild plot slope is equal to 1, pA_2 adequately represents $pKB^{35,36}$. A two-tailed one-sample t-test was used to determine whether the slope of the Schild plot differed significantly from 1.

In vivo plasma half-lives of lipidated hαCGRP8-37 analogues were estimated with non-compartmental analysis by PKSolver. Half-live calculations were based on plasma levels of each compound at 1 h, 6 h and 24 h post dosing.

Data is presented as mean and range in in vitro experiments and mean and SEM in ex vivo experiments. For statistical comparisons, IC50 values between the two antagonists presented in Fig. 9 were compared with a two-tailed unpaired t-test. A One-Way ANOVA with Tukey's multiple comparisons test was used to compare pA_2 values and Schild slopes presented in Table 1. Statistical significance was determined at a p value of <0.05 in all statistical tests.

Results

Effect of acylation length and position on antagonism of hαCGRP8-37

A series of crude hαCGRP8-37 analogues were conjugated with either C18 diacid (DA) or C20DA and varying combinations of linker moieties, including L-γ-glutamyl (γGlu) and 3,8-dioxa-amino-octanoic acid (OEG). Purity of conjugated hαCGRP8-37 analogues ranged between 30 and 50%. Protractors were attached to the epsilon nitrogen of lysines in all positions or at the N-terminal. The resulting peptides library consisted of 190 peptides and was screened in antagonist mode against the hCGRP-R in vitro. The relationship between pIC_{50} , lipidation moiety and lipidation position is presented in Fig. 1. Lipidation of hαCGRP8-37 at all positions were associated with loss of potency on the hCGRP-R (Fig. 1). Positions least susceptible to potency loss were 8, 9, 14, 17, 19, 20, 25, 28 (2–8 fold reduction) with position 14 and position 25 exhibiting the lowest loss of potency (2 and 4 fold reduction). Positions most susceptible to potency loss included 29–33, 36 and 37 (50–500 potency reduction) (Fig. 1).

Based on the lipidation scan, 10 lipidated hαCGRP8-37 analogues were purified to >95%. The selected peptides were conjugated in position 14, 17, 19, 20 and 25 with C18DA-γGlu or C20DA-γGlu (Fig. 2a–e). Antagonism of purified hαCGRP8-37 analogues was subsequently studied. cAMP inhibition curves for the lipidated hαCGRP8-37 analogues are presented in Fig. 2a–e and a cAMP inhibition curve for non-lipidated hαCGRP8-37 is presented in Fig. 2f.

Protraction at position 14, 20 and 25 generated the most potent lipidated hαCGRP8-37 analogues (Fig. 2). Peptides conjugated with C20DA-γGlu were 2–6 fold more potent than C18DA-γGlu protractions at same positions (Fig. 2a–e). An overview of the primary structures of the hαCGRP8-37 analogues with associated IC50 values is presented in Fig. 3.

Half-lives of hαCGRP8-37 analogues are affected by lipidation position

Five hαCGRP8-37 analogues conjugated with C20DA-γGlu at position 14, 17, 19, 20, or 25 were analysed for in vivo exposure in male NMRI mice. All hαCGRP8-37 analogues had detectable plasma levels 24 h post IV-injection. Plasma exposure for all compounds is presented in Fig. 4a and plasma exposure normalized to peak plasma concentrations is presented in Fig. 4b. Associated half-lives are presented in figure legends. An overview of the primary structures of the hαCGRP8-37 analogues with associated half-lives is presented in Fig. 5. Peptides conjugated with C20DA-γGlu at position 14, 17 and 19 had half-lives of 10.1 h, 12.3 h, and 13.7 h, respectively. Shorter half-lives were observed for hαCGRP8-37 derivatives conjugated with C20DA-γGlu at position 20 and 25. At position 20, half-life was 7.5 h. At position 25, half-life was 7.3 h.

Metabolite analysis indicate distinct in vivo degradation patterns between hαCGRP8-37^{S19K-C20DA-γGlu} and hαCGRP8-37^{N25K-C20DA-γGlu}

Next, we compared metabolites derived from the lipidated hαCGRP8-37 analogue with the longest half-life, hαCGRP8-37^{S19K-C20DA-γGlu} and the shortest half-life, hαCGRP8-37^{N25K-C20DA-γGlu}. Identified metabolites are presented in Fig. 6a and b with estimated abundance.

Nine metabolites were identified for hαCGRP8-37^{S19K-C20DA-γGlu} (Fig. 6a). The identified metabolites consisted of four N-terminal fragments (hαCGRP8-36, hαCGRP8-24, hαCGRP8-26 and hαCGRP8-34), three C-terminal fragments (hαCGRP9-37, hαCGRP17-37, and hαCGRP10-37) and two internal fragments (hαCGRP9-36, hαCGRP9-26).

Fourteen metabolites from hαCGRP8-37^{N25K-C20DA-γGlu} were identified (Fig. 6b). These metabolites consisted of two N-terminal fragments (hαCGRP8-35 and hαCGRP8-36), seven C-terminal fragments (hαCGRP9-37,

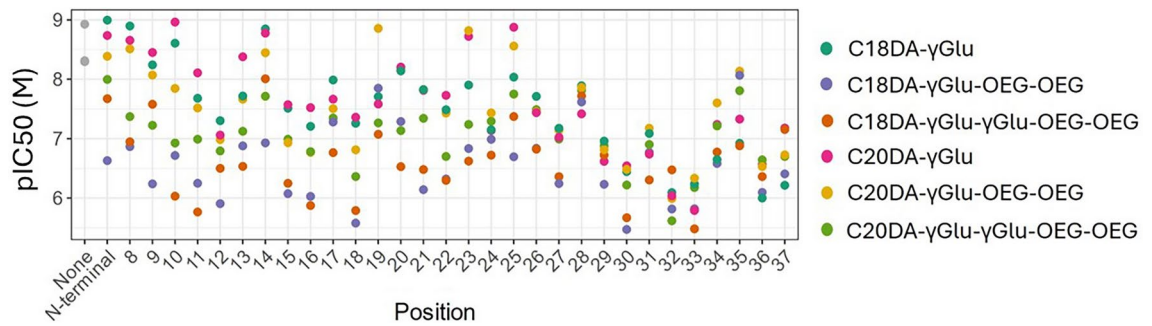


Fig. 1. Overview of the effect of lipidation position and moiety on potency of lipidated haCGRP8-37 analogues. Six different lipidation moieties were applied to a lysine substitution at every amino acid residue of haCGRP8-37. A γ Glu linker was incorporated between the peptide and the connected C18DA or C20DA. The peptides were incubated with a fixed concentration of haCGRP8-37 corresponding to its EC90 (24 pM). Five-point concentration response curves were generated with antagonist concentrations of 30 nM, 100 nM, 300 nM, 1 μ M and 3 μ M. Antagonist potency was estimated as pIC50, which refer to the logarithmic concentration of antagonist required to induce 50% inhibition of the cAMP levels generated from the fixed concentration of haCGRP8-37. Datapoints represent technical replicates from a single independent experiment ($n = 1$).

haCGRP15-37, haCGRP16-37, haCGRP17-37, haCGRP18-37, haCGRP19-37 and haCGRP20-37), and five internal fragments (haCGRP9-36, haCGRP11-18, haCGRP 15-36, haCGRP17-36 and haCGRP18-36).

The C-terminal fragment, haCGRP9-37, was identified from both haCGRP8-37_{N25K-C20DA- γ Glu} and haCGRP8-37_{S19K-C20DA- γ Glu}.

Competitive antagonism of haCGRP8-37 is maintained with N25K-C20DA- γ Glu

The most potent lipidated haCGRP8-37 analogue, haCGRP8-37_{N25K-C20DA- γ Glu}, was selected for further optimization. Schild regression analysis was used to compare antagonism of haCGRP8-37 and haCGRP8-37_{N25K-C20DA- γ Glu} (Fig. 7a–d). pA_2 was 8.23 ± 0.11 for haCGRP8-37 and 8.33 ± 0.29 for haCGRP8-37_{N25K-C20DA- γ Glu}. The Schild slope was 0.94 ± 0.15 for haCGRP8-37 and 0.98 ± 0.15 for haCGRP8-37_{N25K-C20DA- γ Glu}. No significant differences were observed between pA_2 values ($p = 0.933$) or Schild slopes ($p = 0.993$). Both antagonists showed classical competitive antagonism since, there was no effect on α CGRP E_{max} , and the Schild plot slopes did not differ significantly from 1 (haCGRP8-37: $p = 0.370$, haCGRP8-37_{N25K-C20DA- γ Glu}: $P = 0.787$).

Antagonism of haCGRP8-37_{N25K-C20DA- γ Glu} is increased with A36S

haCGRP8-37_{N25K-C20DA- γ Glu} was subjected to an amino acid substitution scan to identify substitutions that enhance antagonism against the hCGRP-R (Fig. 8). A peptide library was designed where all positions were systematically substituted into five different amino acids representing different physicochemical properties. The introduced amino acids were lysine (K), glutamate (E), phenylalanine (F), Threonine (T), or alanine (A). Glycine (G) was introduced, if any of the above residues were natively present. The library consisted of a total of 950 peptides where each peptide had 1–5 substitutions relative to native haCGRP8-37. All peptides were screened for hCGRP-R antagonism and a random forest model was trained to determine the relationship between pIC50 and the amino acid sequence of the peptides. From this model, SHapley Additive exPlanation (SHAP) values were computed to determine the level of contribution of each substitution³⁷. Substitutions with positive SHAP values increased potency, while substitutions with negative SHAP values decreased potency. From the SHAP values it was observed that substitutions in the N-terminal part of the peptide in general had small effects on potency, while substitutions in the C-terminal showed larger effects. The A36S mutation proved to have a large positive SHAP value, indicating a positive effect on pIC50 of haCGRP8-37_{N25K-C20DA- γ Glu} (Fig. 8).

To confirm the positive contribution of A36S, haCGRP8-37_{N25K-C20DA- γ Glu} and haCGRP8-37_{A36S, N25K-C20DA- γ Glu} were purified to >95% and their potencies against the hCGRP-R was compared (Fig. 9) An unpaired t-test was used to compare pIC50 between haCGRP8-37_{N25K-C20DA- γ Glu} and haCGRP8-37_{A36S, N25K-C20DA- γ Glu}. pIC50 for haCGRP8-37_{A36S, N25K-C20DA- γ Glu} was significantly lower than for haCGRP8-37_{N25K-C20DA- γ Glu} (7.51 ± 0.21 vs 8.14 ± 0.33 , $p < 0.001$).

The combination of A36S and N25K-C20DA- γ Glu increases the Schild slope of haCGRP8-37

To gain further understanding of the A36S mutation, we used Schild regression analysis to study how the A36S mutation affects antagonism of haCGRP8-37 with and without N25K-C20DA- γ Glu conjugation (Fig. 10a,b). Results are presented in Table 1 with results from the previous Schild analyses of haCGRP8-37 and haCGRP8-37_{N25K-C20DA- γ Glu}.

pA_2 for haCGRP8-37_{A36S} was significantly higher than pA_2 for haCGRP8-37 (8.78 ± 0.42 vs 8.23 ± 0.11 , $p = 0.038$). pA_2 for haCGRP8-37_{A36S} was also significantly higher than pA_2 for haCGRP8-37_{A36S, N25K-C20DA- γ Glu} (8.78 ± 0.42 vs 8.17 ± 0.50 , $p = 0.021$).

Comparison of Schild slopes showed that haCGRP8-37_{A36S, N25K-C20DA- γ Glu} displayed a significantly higher Schild slope than haCGRP8-37 (1.83 ± 0.63 vs 0.94 ± 0.15 , $p < 0.001$), haCGRP8-37_{A36S} (1.83 ± 0.63 vs 1.08 ± 0.23 ,

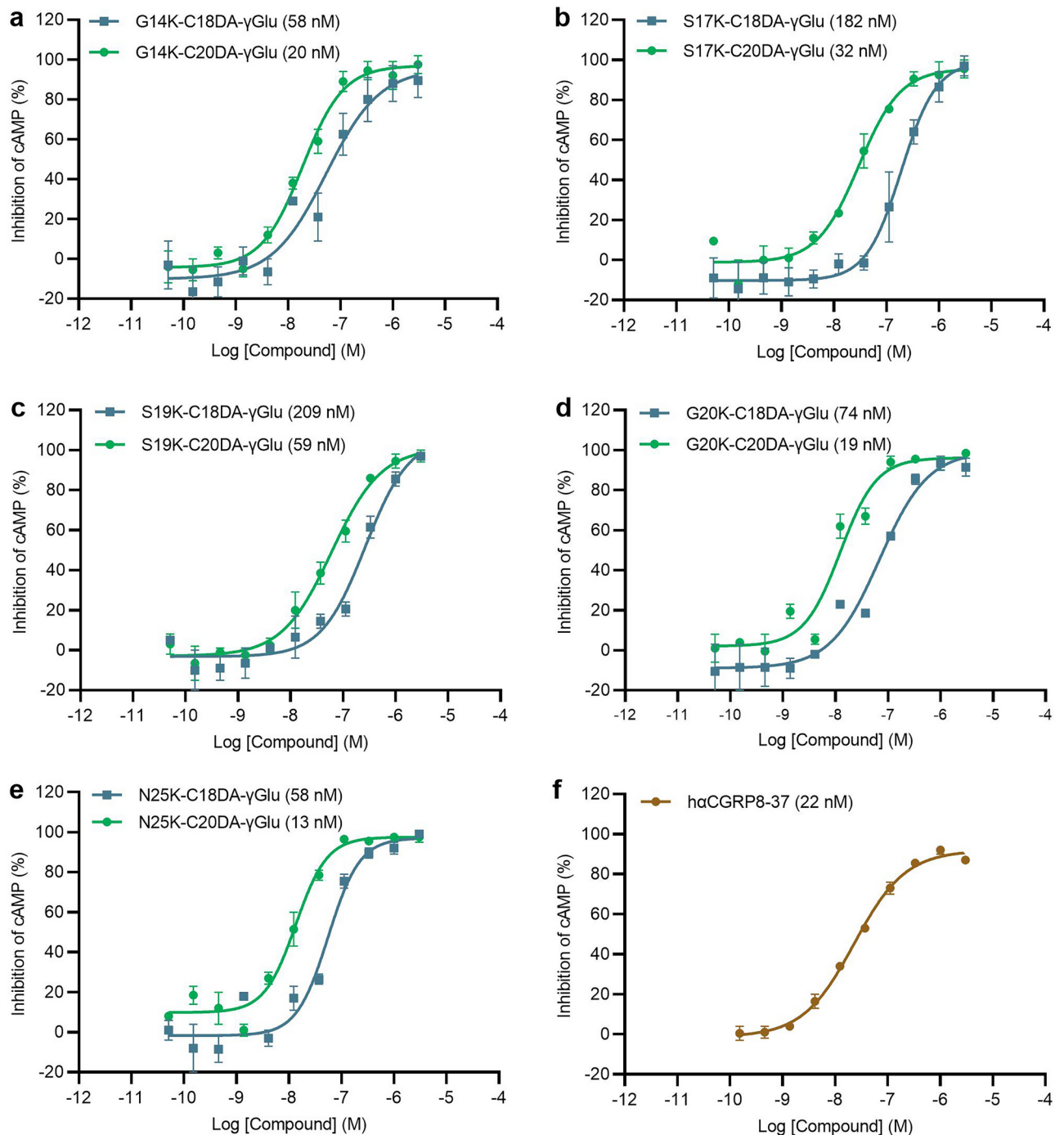


Fig. 2. cAMP inhibition curves of lipidated haCGRP8-37 analogues conjugated with either C18DA-γGlu or C20DA-γGlu at position 14 (a), 17 (b), 19 (c), 20 (d) and 25 (e) and non-lipidated haCGRP8-37 (f). CHO-K1 cells expressing the hCGRP-R were exposed to increasing concentrations of antagonist and a fixed concentration of haCGRP corresponding to EC90 (24 pM). Data points are presented as mean and range of $n = 2$. Experiments were performed in singulates. Mean IC50 values are presented in figure legends.

$p = 0.003$), and haCGRP8-37_{N25K-C20DA-γGlu} (1.83 ± 0.63 vs 0.94 ± 0.15 , $p < 0.001$). The Schild slope for haCGRP8-37_{A36S, N25K-C20DA-γGlu} was significantly higher than 1 ($p = 0.044$). The Schild slope for haCGRP8-37_{A36S} was not significantly different from 1 ($p = 0.336$).

haCGRP8-37_{N25K-C20DA-γGlu} and haCGRP8-37_{A36S, N25K-C20DA-γGlu} antagonize haCGRP-induced relaxation of rat mesenteric arteries

Wire myography was applied to study antagonism of haCGRP8-37_{N25K-C20DA-γGlu} and haCGRP8-37_{A36S, N25K-C20DA-γGlu} against haCGRP-induced relaxation of rat mesenteric arteries. Arteries were incubated

Peptide sequence	Lipidation at γ Glu	Lipidation position	EC ₅₀ (nM)
	C18DA	14	58
	C18DA	17	182
	C18DA	19	209
	C18DA	20	74
	C18DA	25	58
	C20DA	14	20
	C20DA	17	32
	C20DA	19	59
	C20DA	20	19
	C20DA	25	13

Fig. 3. Overview of purified haCGRP8-37 analogues with associated IC₅₀ values. Results are presented as mean of $n = 2$. Created with BioRender.com.

without antagonist or with a fixed concentration of antagonist (10–300 nM). Artery segments were subsequently exposed to progressively increasing concentrations of haCGRP ranging from 1 pM to 3 μ M (Fig. 11a,b).

EC₅₀_{haCGRP} values in the presence of 10 nM, 30 nM, 100 nM and 300 nM haCGRP8-37^{N25K-C20DA- γ Glu} and haCGRP8-37^{A36S, N25K-C20DA- γ Glu} is presented in Table 2 with EC₅₀_{haCGRP} of the associated control artery segments. Schild plots were subsequently generated for both antagonists and pA₂ and Schild slopes were estimated with associated 95% CI (Fig. 11c). For haCGRP8-37^{N25K-C20DA- γ Glu}, pA₂ was 7.91 (95% CI = 7.65 to 8.53) and the Schild slope was 1.06 (95% CI = 0.66 to 1.50). For haCGRP8-37^{A36S, N25K-C20DA- γ Glu}, pA₂ was 8.15 (95% CI = 7.97 to 8.39) and Schild slope was 1.29 (95% CI = 1.02 to 1.55).

Discussion

In this present study, we used the streamLine platform to explore lipidation in haCGRP peptide-based migraine therapeutics. We recently used the streamLine platform to develop a potent and long-lasting GLP-1 receptor agonist based on secretin³³. In this present study, the streamLine platform was used to synthesize and characterize a wide series of lipidated haCGRP8-37.

First, a series of lipidated haCGRP8-37 analogues were screened for their antagonism against the hCGRP-R. Next, a subset of haCGRP8-37 analogues conjugated with C20DA- γ Glu at varying positions was analysed for in vivo exposure in mice. Here, several observations were made of how lipidation length and position affect potency and in vivo exposure of tested lipidated haCGRP8-37 analogues. However, definitive conclusion regarding potency and in vivo exposure are limited due to small sample sizes ($n = 1-2$) in these initial screening processes.

A general observation was that greatest losses of potency occurred when the lipidation was positioned in the C-terminal region of haCGRP8-37, being consistent with a previous study on palmitoylation at K35C, which resulted in a 70-fold reduction of potency²². This effect of lipid positioning may be explained by the two-domain model of class B protein coupled receptors. This model dictates that the C-terminal region of a peptide ligand enables binding to the N-terminal domain of the receptor³⁸.

We also observed that antagonism of lipidated haCGRP8-37 derivatives against the hCGRP-R appeared to be affected by the length of the fatty acid. The relationship between length of the fatty acid and potency has been extensively studied for glucagon-like peptide 1 (GLP-1) analogues, where increased length of the fatty acid is associated with reductions in GLP-1 receptor agonist potency^{37,39,40}. In contrast, we observed a positive association between length of the fatty acid and antagonist potency of haCGRP8-37. haCGRP8-37 analogues conjugated with C20DA- γ Glu were 2–6 fold more potent than analogues conjugated with C18DA- γ Glu at same positions. This highlights that the relationship between the length of the fatty acid and potency is complex and highly dependent on the specific lipidated peptide. C20DA- γ Glu protraction has previously been observed to extend receptor residence time of amylin analogues and result in a prolonged duration of action⁴¹. Positive effects on antagonism of haCGRP8-37 with C20DA- γ Glu compared to C18DA- γ Glu protraction could be related to a similar mode of action.

Since C20DA- γ Glu conjugations were associated with greater potency compared to C18DA- γ Glu conjugations, five haCGRP8-37 conjugated with C20DA- γ Glu at position 14, 17, 19, 20, and 25 were selected

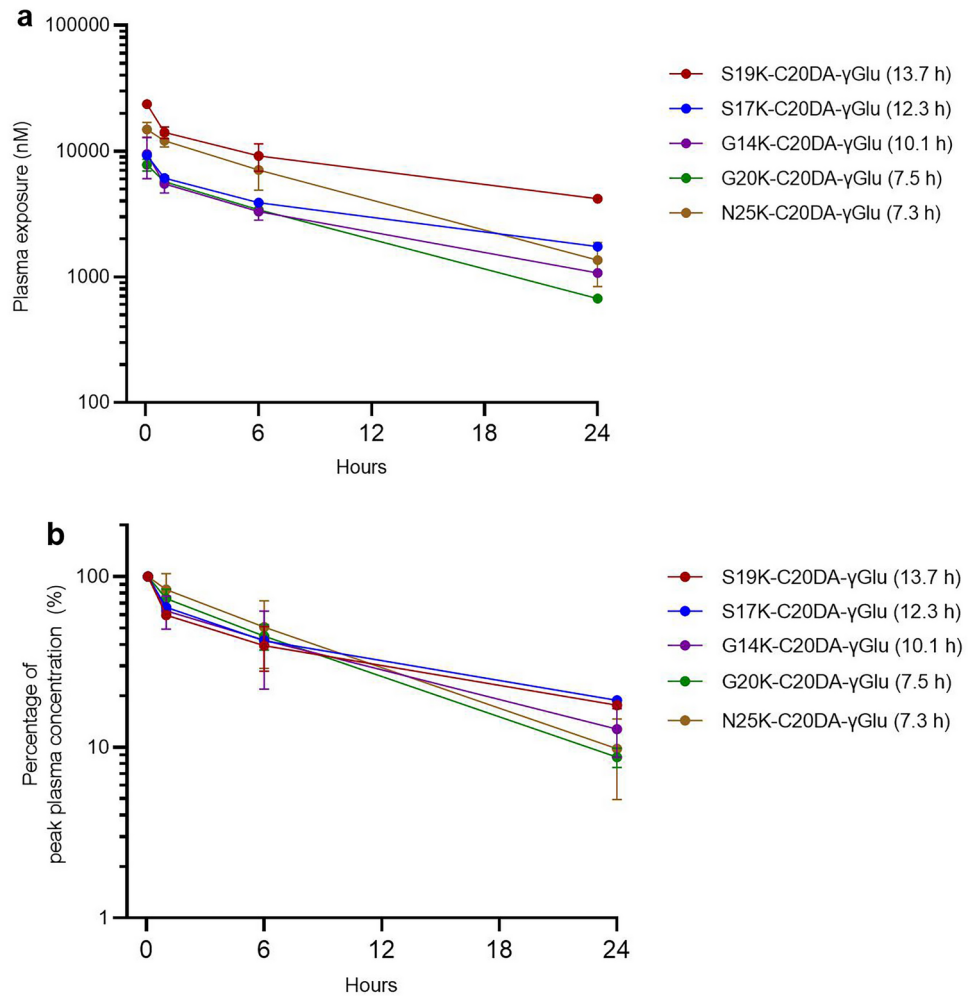


Fig. 4. (a) Plasma exposure and (b) plasma exposure normalised to peak plasma concentrations of haCGRP8-37 analogues conjugated with C20DA-γGlu at position 14, 17, 19, 20 and 25 at 5 min, 1 h, 6 h and 24 h post dosing in male NMRI mice. Data point represent mean and range of $n=2$, except for C20DA-γGlu protraction at position 17 where $n=1$. $T_{1/2}$ for each compound is presented in legends.

Peptide sequence	Lipidation at γGlu	Lipidation position	$T_{1/2}$ (hours)
Y T H R L A K L L S R S G G V V X N N F V P T N Y G S K A F C20DA-γGlu	C20DA	14	10.1
Y T H R L A G L L K R S G G V V X N N F V P T N Y G S K A F C20DA-γGlu	C20DA	17	12.3
Y T H R L A G L L S R K G G V V X N N F V P T N Y G S K A F C20DA-γGlu	C20DA	19	13.7
Y T H R L A G L L S R S K G V V X N N F V P T N Y G S K A F C20DA-γGlu	C20DA	20	7.5
Y T H R L A G L L S R S G G V V K N F V P T N Y G S K A F C20DA-γGlu	C20DA	25	7.3

Fig. 5. Overview of purified haCGRP8-37 analogues with associated and half-lives. Results are presented as mean of $n=2$, except for C20DA-γGlu protraction at position 17 where $n=1$. Created with BioRender.com.

for exposure analysis in mice. All lipidated haCGRP8-37 analogues had detectable plasma levels 24 h post administration, which highlights that C20DA-γGlu conjugation can extend half-life of haCGRP8-37.

The ~6 h difference between haCGRP8-37_{S19K-C20DA-γGlu} and haCGRP8-37_{N25K-C20DA-γGlu} indicate that in vivo degradation of haCGRP8-37 is affected by the position of the C20DA-γGlu conjugation. To study if the

haCGRP8-37 _{S19K-C20DA-γGlu}				
Sequence	Full length	Abundance	Abundance	Abundance
		1 hour	6 hours	24 hours
N-terminal fragments				
8-36	VTHRLAGLLSRK*GGVRRNFVPTNVSQAF-NH2	< 0.001	0.014	0.069
8-24	VTHRLAGLLSRK*GGVRR	0.013	0.022	0.018
8-26	VTHRLAGLLSRK*GGVRRKN	0.040	0.082	0.163
8-34	VTHRLAGLLSRK*GGVRRNFVPTNVS	NA	0.013	0.067
C-terminal fragments				
9-37	THRLAGLLSRK*GGVRRNFVPTNVSQAF-NH2	0.027	0.197	0.995
17-37	SRK*GGVRRNFVPTNVSQAF-NH2	0.242	0.057	0.225
10-37	HRLAGLLSRK*GGVRRNFVPTNVSQAF-NH2	< 0.01	0.034	0.152
Internal fragments				
9-36	THRLAGLLSRK*GGVRRNFVPTNVSQAF	NA	< 0.001	0.067
9-26	THRLAGLLSRK*GGVRRKN	< 0.001	0.043	0.344

haCGRP8-37 _{N25K-C20DA-γGlu}				
Sequence	Full length	Abundance	Abundance	Abundance
		1 hour	6 hours	24 hours
N-terminal fragments				
8-36	VTHRLAGLLSRSGGVRRK*NFVPTNVSQAF-NH2	0.020	0.117	0.470
8-35	VTHRLAGLLSRSGGVRRK*NFVPTNVSQR	0.039	0.013	0.030
C-terminal fragments				
9-37	THRLAGLLSRSGGVRRK*NFVPTNVSQAF-NH2	0.051	0.440	2.030
15-37	LLSRSGGVRRK*NFVPTNVSQAF-NH2	0.073	0.721	3.880
10-37	LSRSGGVRRK*NFVPTNVSQAF-NH2	0.013	0.129	0.740
17-37	SRSGGVRRK*NFVPTNVSQAF-NH2	0.086	0.711	14.200
18-37	RSRSGGVRRK*NFVPTNVSQAF-NH2	0.037	0.076	0.970
19-37	SGGVRRK*NFVPTNVSQAF-NH2	1.444	1.933	4.450
20-37	GGVRRK*NFVPTNVSQAF-NH2	0.151	0.181	3.990
Internal fragments				
19-36	SGGVRRK*NFVPTNVSQAF	NA	0.338	3.630
11-18	RLAGLLSR	0.311	0.274	0.560
15-36	LLSRSGGVRRK*NFVPTNVSQAF	0.029	0.241	1.210
17-36	SRSGGVRRK*NFVPTNVSQAF	NA	0.093	3.790
18-36	RSRSGGVRRK*NFVPTNVSQAF	NA	0.014	0.370

Fig. 6. Metabolites from (a) haCGRP8-37_{S19K-C20DA-γGlu} and (b) haCGRP8-37_{N25K-C20DA-γGlu}. **K*** refers to the lysine residue where the C20DA-γGlu is positioned. Abundance was estimated as the ratio of metabolite-EIC relative to EIC of the intact peptide. For each timepoint, the most abundant metabolites are highlighted by a progressive increase in colour intensity. Results are presented as mean of $n = 2$.

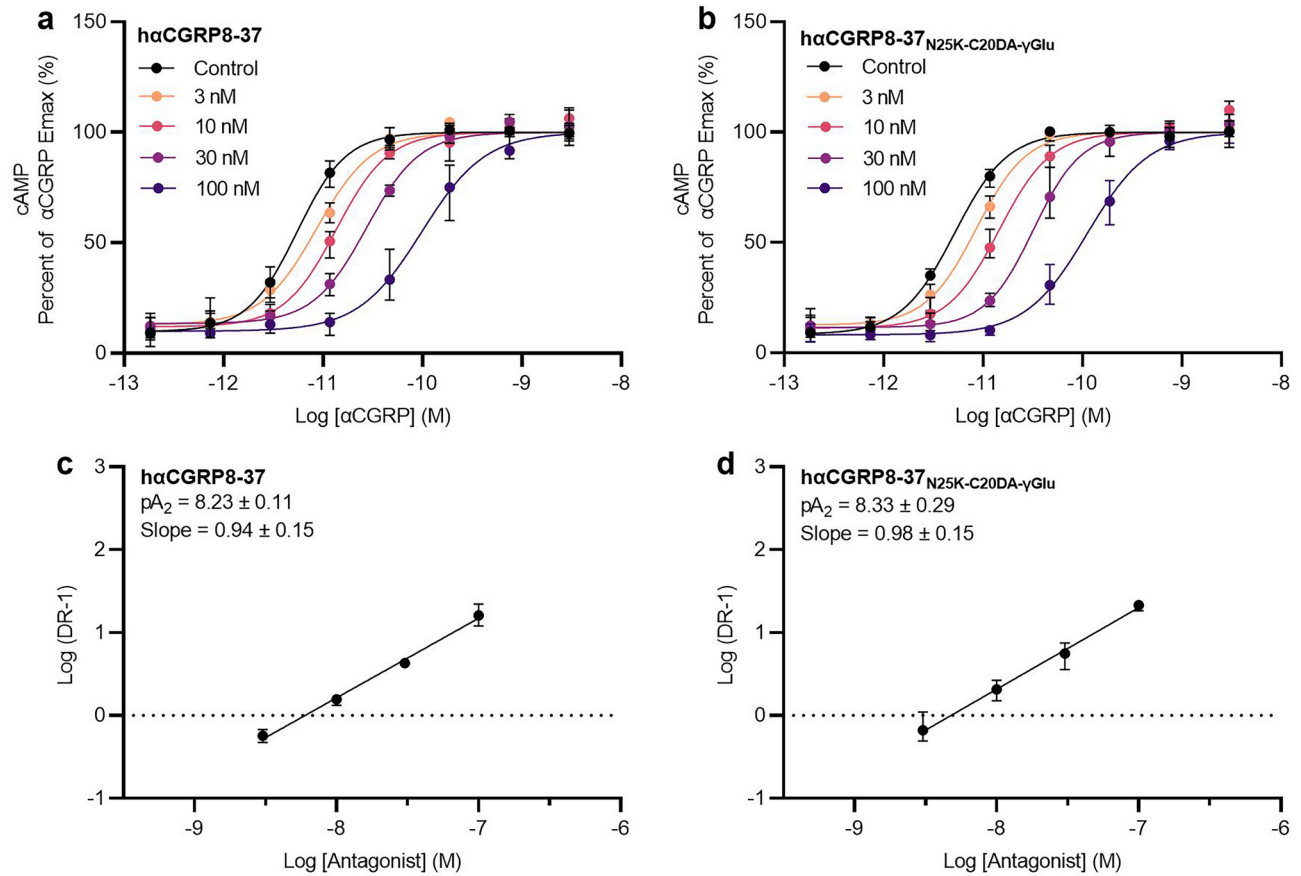


Fig. 7. Inhibition of haCGRP-stimulated cAMP generation in CHO-K1 expressing the hCGRP-R. Concentration–response curves were generated in the absence or presence of (a) haCGRP8-37 or (b) haCGRP8-37_{N25K-C20DA-γGlu}. (c) Schild plot of haCGRP8-37 and (d) Schild plot of haCGRP8-37_{N25K-C20DA-γGlu}. Experiments were performed in duplicates. Results are presented as mean ± range of $n = 3$.

positioning of the C20DA-γGlu affects in vivo degradation of haCGRP8-37, we compared metabolites derived from haCGRP8-37_{S19K-C20DA-γGlu} and haCGRP8-37_{N25K-C20DA-γGlu} at 1 h, 6 h and 24 h post injection. The C-terminal fragment haCGRP9-37 was identified for both analogues, which suggests that both peptides are susceptible to N-terminal truncation at the V8 residue.

Comparisons of metabolites derived from haCGRP8-37_{S19K-C20DA-γGlu} and haCGRP8-37_{N25K-C20DA-γGlu} suggests that the positioning of the C20DA-γGlu conjugation influences in vivo degradation of haCGRP8-37.

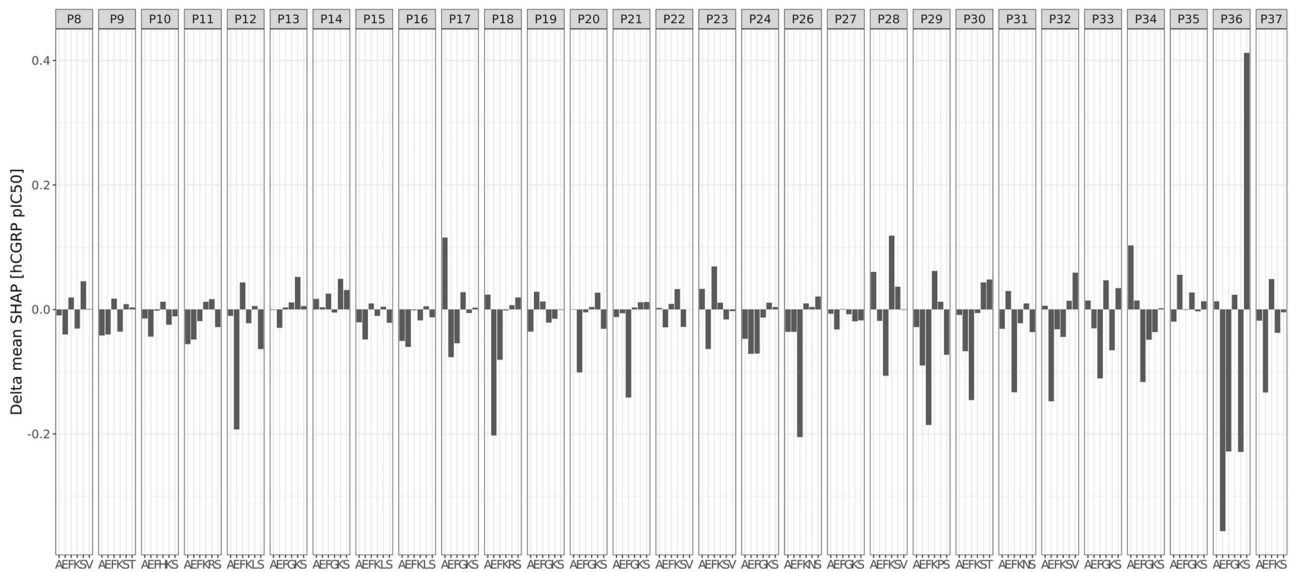


Fig. 8. Contribution of amino acid positions in haCGRP8-37_{N25K-C20DA-γGlu} for antagonism against the hCGRP-R expressed in the CHO-K1 cell line. Cells were incubated with 24 pM haCGRP (EC90) and increasing concentrations of antagonist. Antagonist potency was evaluated with five-point antagonist concentration response curves ranging from 30 nM to 3 μM. Each position was mutated to five different amino acids, either alone or in combination, resulting in a total data set consisting of 950 peptides. Lysine (K), glutamic acid (E), phenylalanine (F), serine (S), and alanine (A) were applied as substitutions. When one of these amino acids was already present in the backbone, a glycine (G) was induced as alternative. A random forest model was computed based on the relationship between the pIC50 values and the amino acid sequences. SHAP values were computed to determine the potency contribution of each mutation, where a positive SHAP value correspond to a positive contribution and a negative SHAP value corresponds to a negative contribution.

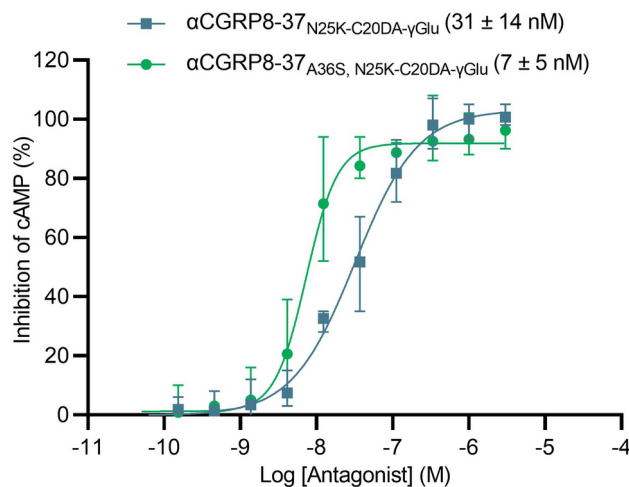


Fig. 9. cAMP inhibition curves of haCGRP8-37_{N25K-C20DA-γGlu} and haCGRP8-37_{A36S, N25K-C20DA-γGlu}. CHO-K1 cells expressing the hCGRP-R were exposed to increasing concentrations of antagonist and a fixed concentration of haCGRP corresponding to its EC90 (24 pM). Experiments were performed in singlicates. Data points are presented as mean ± range of $n = 5$. IC50 values are presented in figure legends as mean ± range.

Seven C-terminal fragments were identified from haCGRP8-37_{N25K-C20DA-γGlu}. These included haCGRP15-37, haCGRP16-37, haCGRP17-37, haCGRP18-37, haCGRP19-37 and haCGRP20-37, with haCGRP17-37 and haCGRP19-37 being the most abundant. The identification of these metabolites suggests that the LLSR motif of haCGRP8-37_{N25K-C20DA-γGlu} is susceptible to degradation in vivo. Interestingly, the lower abundance of C-terminal fragments identified from haCGRP8-37_{S19K-C20DA-γGlu} compared to haCGRP8-37_{N25K-C20DA-γGlu} suggest that positioning the C20DA-γGlu conjugation within the LLSR motif offer greater protection against in vivo cleavage in this region.

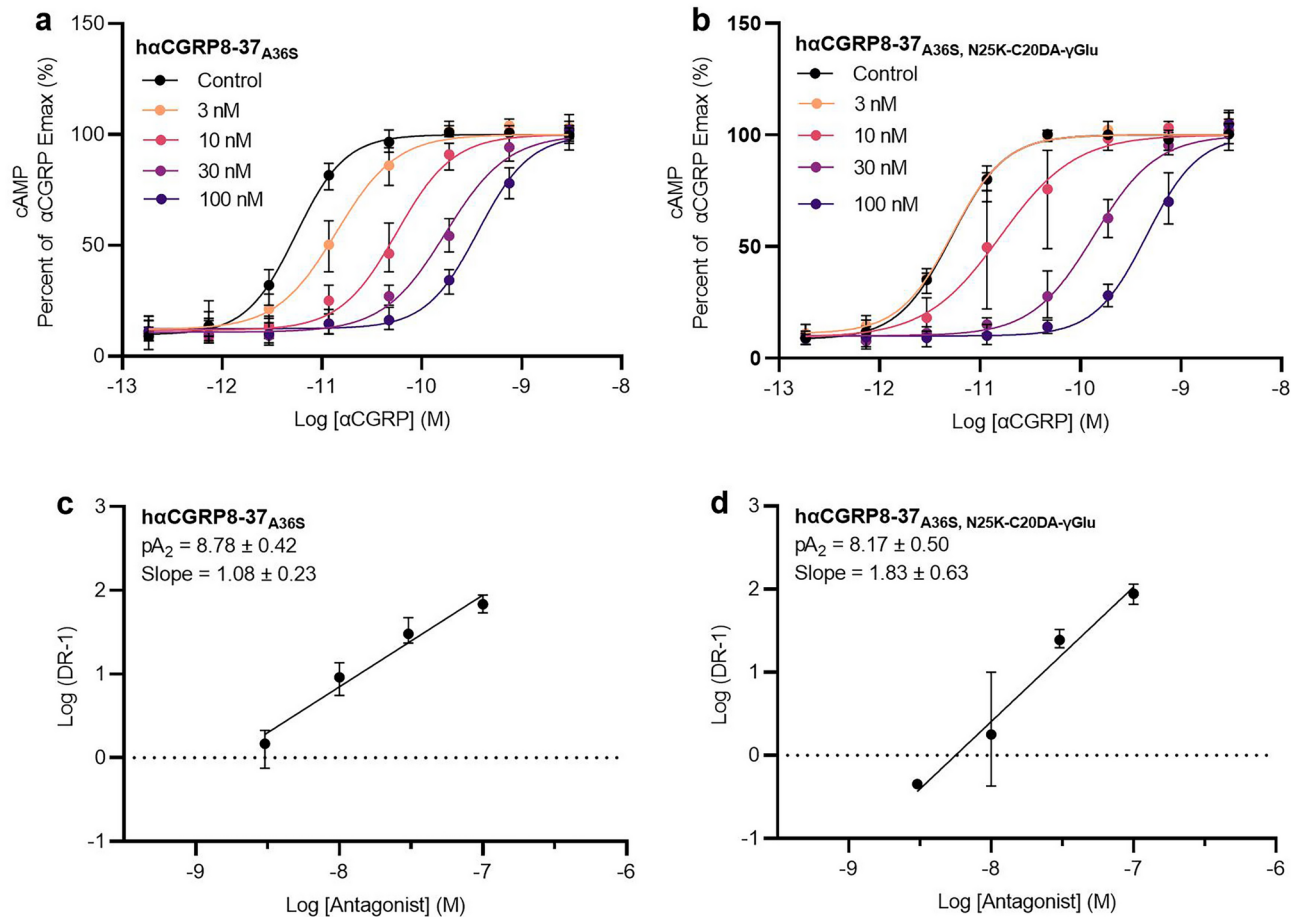


Fig. 10. Inhibition of h αCGRP -stimulated cAMP generation in CHO-K1 expressing the h CGRP-R . Concentration–response curves were generated in the absence or presence of (a) h $\alpha\text{CGRP8-37}_{\text{A36S}}$ or (b) h $\alpha\text{CGRP8-37}_{\text{A36S, N25K-C20DA-}\gamma\text{Glu}}$. (c) Schild plot of h $\alpha\text{CGRP8-37}_{\text{A36S}}$ and (d) Schild plot of h $\alpha\text{CGRP8-37}_{\text{A36S, N25K-C20DA-}\gamma\text{Glu}}$. Experiments were performed in duplicates. Results are presented as mean \pm range of $n = 3$.

	pA_2	Schild slope
h $\alpha\text{CGRP8-37}$ No modifications	8.23 ± 0.11	0.94 ± 0.15
h $\alpha\text{CGRP8-37}$ A36S	8.78 ± 0.42	1.08 ± 0.23
h $\alpha\text{CGRP8-37}$ N25K-C20DA- γGlu	8.33 ± 0.29	0.98 ± 0.15
h $\alpha\text{CGRP8-37}$ A36S, N25K-C20DA- γGlu	8.17 ± 0.50	1.83 ± 0.53

Table 1. Results from Schild regression analyses. Experiments were performed in duplicates. Results are presented as mean \pm range of $n = 3$.

Moreover, metabolites identified from h $\alpha\text{CGRP8-37}_{\text{S19K-C20DA-}\gamma\text{Glu}}$, suggests that the KNN motif of h $\alpha\text{CGRP8-37}$ is also susceptible to in vivo degradation. This is highlighted by the identification of the N-terminal fragments h $\alpha\text{CGRP8-24}$ and h $\alpha\text{CGRP8-26}$ and the internal fragment, h $\alpha\text{CGRP9-26}$. These metabolites were not identified for h $\alpha\text{CGRP8-37}_{\text{N25K-C20DA-}\gamma\text{Glu}}$, which suggests that positioning the C20DA- γGlu conjugation at N25K offer greater protection against cleavage at the KNN motif. A previous study identified two in vivo cleavage sites for endogenous αCGRP located within the LLSR motif and KNN motif, respectively⁴². The ~ 6 h longer half-life of h $\alpha\text{CGRP8-37}_{\text{S19K-C20DA-}\gamma\text{Glu}}$ compared to h $\alpha\text{CGRP8-37}_{\text{N25K-C20DA-}\gamma\text{Glu}}$ suggests that longer half-lives can be obtained by positioning the C20DA- γGlu in proximity to the cleavage site S17-R18 within the LLSR motif.

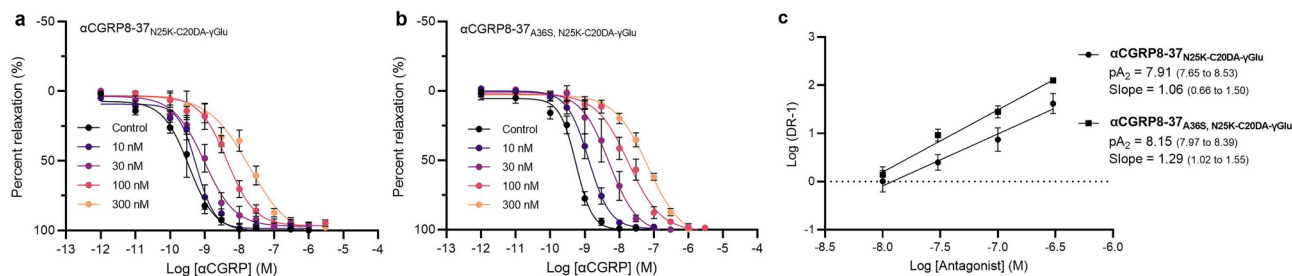


Fig. 11. Inhibition of haCGRP induced relaxation of rat mesenteric arteries with haCGRP8-37_{N25K-C20DA-γGlu} and haCGRP8-37_{A36S, N25K-C20DA-γGlu}. Arteries were exposed to progressively increasing concentrations of haCGRP in the presence or absence of 10 nM, 30 nM, 100 nM and 300 nM (a) haCGRP8-37_{N25K-C20DA-γGlu} or (b) haCGRP8-37_{A36S, N25K-C20DA-γGlu} following a stable contraction induced by 200 nM U4619. (c) Schild plots for haCGRP8-37_{N25K-C20DA-γGlu} and haCGRP8-37_{A36S, N25K-C20DA-γGlu}. Data points are presented as means of 6–8 independent experiments. Experiments were performed in singlicates. Error bars represent SEM.

	haCGRP8-37 _{N25K-C20DA-γGlu}	haCGRP8-37 _{A36S, N25K-C20DA-γGlu}
EC50 _{haCGRP} No antagonist	0.52 ± 0.17 nM (6)	0.60 ± 0.11 (8)
EC50 _{haCGRP} + 10 nM antagonist	0.58 ± 0.16 nM (4)	1.44 ± 0.28 nM (7)
EC50 _{haCGRP} + 30 nM antagonist	2.15 ± 1.21 nM (6)	6.31 ± 1.97 nM (5)
EC50 _{haCGRP} + 100 nM antagonist	4.78 ± 0.88 nM (5)	21.48 ± 6.18 nM (8)
EC50 _{haCGRP} + 300 nM antagonist	19.44 ± 3.42 nM (4)	61.73 ± 6.70 nM (5)

Table 2. EC50_{haCGRP} values generated in the presence of haCGRP8-37_{N25K-C20DA-γGlu} and haCGRP8-37_{A36S, N25K-C20DA-γGlu}. The number of experimental units (*n*) are noted in parentheses. Experiments were performed in singlicates. Data is presented as a mean ± SEM.

haCGRP8-37_{N25K-C20DA-γGlu} was identified as the most potent of the tested lipidated haCGRP8-37 analogues. haCGRP8-37_{N25K-C20DA-γGlu} was therefore selected as backbone for further optimization. Schild regression analysis demonstrated that haCGRP8-37_{N25K-C20DA-γGlu} behaved as a competitive antagonist with similar potency to native haCGRP8-37. The pA₂ of 8.23 for CGRP8-37 is in accordance with other findings^{43–45}. To further improve potency of haCGRP8-37_{N25K-C20DA-γGlu}, we performed an amino acid substitution scan to identify substitutions that further enhance antagonism against the hCGRP-R. Extensive structure activity analyses have previously been performed to truncated haCGRP-analogues^{46,47}, but not in combination with lipidation. We found that A36S significantly reduced IC50 of haCGRP8-37_{N25K-C20DA-γGlu} from 31 to 7 nM, corresponding to an ~4.5-fold gain of potency. A36S has previously been demonstrated to induce a sixfold gain of antagonist potency to haCGRP27-37, possibly through stabilization of its β-turn of CLR in the extra cellular domain of the CGRP receptor⁴⁷. The stabilization of the β-turn by the antagonist appear to be important and shared by gepants and peptide antagonists of CGRP^{47,48}. The possible docking of C-terminal CGRP antagonists to the β-turn is confirmed by crystal structure and EM-CRYO. The A36S possibly strengthen the interaction further by forming hydrogen bonds to CLR G33 and F37^{47,49}.

To study how the A36S mutation affects antagonism of haCGRP8-37 in the presence and absence of N25K-C20DA-γGlu, we used Schild regression analysis to compare haCGRP8-37, haCGRP8-37_{N25K-C20DA-γGlu}, haCGRP8-37_{A36S} and haCGRP8-37_{A36S, N25K-C20DA-γGlu}. We found that haCGRP8-37_{A36S} behaved as a competitive antagonist with a pA₂ of 8.78 and a Schild plot slope of 1.08 that did not differ significantly from 1. However, haCGRP8-37_{A36S, N25K-C20DA-γGlu} displayed a higher Schild plot slope of 1.83, that was also significantly higher than 1. In addition, pA₂ of haCGRP8-37_{A36S, N25K-C20DA-γGlu} was significantly lower than pA₂ for haCGRP8-37_{A36S} (8.17 vs 8.78). In contrast, N25K-C20DA-γGlu to native haCGRP8-37 did not affect pA₂ or Schild slope. This suggests that the combination of A36S and N25K-C20DA-γGlu may influence the binding kinetics of haCGRP8-37 in a manner distinct from the effects of each individual modification. A Schild plot slope higher than 1 can reside from a slow onset of action of the antagonist, which causes pA₂ to underestimate the true pKB^{50,51}. This has previously been observed for the small molecule hCGRP-R antagonist, olcegepant, although this behaviour appears to be cell line dependent⁴⁴. Therefore, future studies should further explore how the A36S mutation and N25K-C20DA-γGlu lipidation affect binding kinetics of haCGRP8-37.

The final aim of this study was to analyse antagonism of lipidated haCGRP8-37 analogues ex vivo. Here, we used wire myography to study antagonism of haCGRP8-37_{N25K-C20DA-γGlu} and haCGRP8-37_{A36S, N25K-C20DA-γGlu} against haCGRP-induced vasodilation. Wire myography is commonly used to study vasodilative effects of

haCGRP and has been used to characterize several CGRP-R antagonists^{52–56}. In this present study, vascular measurements were performed in rat mesenteric arteries since they densely express the CGRP-R and are known to be responsive to α CGRP^{54,55,57}. Therefore, vascular measurement of rat mesenteric arteries is an easily accessible method for studying α CGRP physiology. Although haCGRP8-37_{A36S, N25K-C20DA- γ Glu} was generally observed to induce greater dose-shifts in the haCGRP concentration–response curve, especially at antagonist concentrations of 100 nM and 300 nM, pA₂ values derived from the Schild regression analyses did not demonstrate any significant difference in potency between the two lipidated analogues.

In conclusion, we demonstrate a pipeline for development of vasoactive lipidated haCGRP peptide antagonists. We highlight benefits by increasing the lipid length to conjugated haCGRP8-37 analogues, and that lipidation at the LLSR motif may lead to superior half-lives compared to positions further towards the C-terminus. Finally, our results demonstrate that A36S can improve antagonism of a lipidated haCGRP8-37 analogue. However, future studies should further seek to explore how binding kinetics of haCGRP8-37 is affected by the combination of A36S and N25K-C20DA- γ Glu. In conclusion, this study supports development of lipidated hCGRP-R antagonist as potential migraine therapeutics.

Data availability

Access to datasets generated during the current study are available upon reasonable request to the corresponding author.

Received: 28 August 2024; Accepted: 24 December 2024

Published online: 13 January 2025

References

- Zaidi, M. et al. Structure-activity relationship of human calcitonin-gene-related peptide. *Biochem. J.* **269**(3), 775–780 (1990).
- Russell, F. A. et al. Calcitonin gene-related peptide: Physiology and pathophysiology. *Physiol. Rev.* **94**(4), 1099–1142 (2014).
- Mulderry, P. K. et al. Differential expression of alpha-CGRP and beta-CGRP by primary sensory neurons and enteric autonomic neurons of the rat. *Neuroscience* **25**(1), 195–205 (1988).
- Edvinsson, L. Role of CGRP in migraine. *Handb. Exp. Pharmacol.* **255**, 121–130 (2019).
- Cottrell, G. S. CGRP receptor signalling pathways. *Handb. Exp. Pharmacol.* **255**, 37–64 (2019).
- Lima, W. G. et al. Role of calcitonin gene-related peptide in energy metabolism. *Endocrine* **58**(1), 3–13 (2017).
- Favoni, V. et al. CGRP and migraine from a cardiovascular point of view: what do we expect from blocking CGRP?. *J. Headache Pain* **20**(1), 27 (2019).
- Iyengar, S., Ossipov, M. H. & Johnson, K. W. The role of calcitonin gene-related peptide in peripheral and central pain mechanisms including migraine. *Pain* **158**(4), 543–559 (2017).
- Haanes, K. A. & Edvinsson, L. Pathophysiological mechanisms in migraine and the identification of new therapeutic targets. *CNS Drugs* **33**(6), 525–537 (2019).
- Melo-Carrillo, A. et al. Fremanezumab-A humanized monoclonal anti-CGRP antibody-inhibits thinly myelinated (Adelta) but not unmyelinated (C) meningeal nociceptors. *J. Neurosci.* **37**(44), 10587–10596 (2017).
- Zhang, L. et al. Role of intraganglionic transmission in the trigeminovascular pathway. *Mol. Pain* **15**, 1744806919836570 (2019).
- Moore, E. L. & Salvatore, C. A. Targeting a family B GPCR/RAMP receptor complex: CGRP receptor antagonists and migraine. *Br. J. Pharmacol.* **166**(1), 66–78 (2012).
- Negro, A. & Martelletti, P. Gepants for the treatment of migraine. *Expert Opin. Investig. Drugs* **28**(6), 555–567 (2019).
- Goadsby, P. J. et al. Efficacy and safety of erenumab (AMG334) in episodic migraine patients with prior preventive treatment failure: A subgroup analysis of a randomized, double-blind, placebo-controlled study. *Cephalalgia* **39**(7), 817–826 (2019).
- Shi, L. et al. Pharmacologic characterization of AMG 334, a potent and selective human monoclonal antibody against the calcitonin gene-related peptide receptor. *J. Pharmacol. Exp. Ther.* **356**(1), 223–231 (2016).
- Nahas, S. J. et al. Efficacy and safety of fremanezumab in clinical trial participants aged ≥ 60 years with episodic or chronic migraine: Pooled results from 3 randomized, double-blind, placebo-controlled phase 3 studies. *J. Headache Pain* **22**(1), 141 (2021).
- Goadsby, P. J. & Edvinsson, L. The trigeminovascular system and migraine: Studies characterizing cerebrovascular and neuropeptide changes seen in humans and cats. *Ann. Neurol.* **33**(1), 48–56 (1993).
- Durham, P. L. & Russo, A. F. Regulation of calcitonin gene-related peptide secretion by a serotonergic antimigraine drug. *J. Neurosci.* **19**(9), 3423–3429 (1999).
- Miranda, L. P. et al. Identification of potent, selective, and metabolically stable peptide antagonists to the calcitonin gene-related peptide (CGRP) receptor. *J. Med. Chem.* **51**(24), 7889–7897 (2008).
- Miranda, L. P. et al. Peptide antagonists of the calcitonin gene-related peptide (CGRP) receptor with improved pharmacokinetics and pharmacodynamics. *Biopolymers* **100**(4), 422–430 (2013).
- Srinivasan, K. et al. Pharmacological, pharmacokinetic, pharmacodynamic and physicochemical characterization of FE 205030: A potent, fast acting, injectable CGRP receptor antagonist for the treatment of acute episodic migraine. *J. Pharm. Sci.* **111**(1), 247–261 (2022).
- Jamaluddin, A. et al. Lipidated calcitonin gene-related peptide (CGRP) peptide antagonists retain CGRP receptor activity and attenuate CGRP action in vivo. *Front. Pharmacol.* **13**, 832589 (2022).
- Killoran, P. M. et al. Novel peptide calcitonin gene-related peptide antagonists for migraine therapy. *J. Pharm. Pharmacol.* **75**(12), 1581–1589 (2023).
- Wang, L. et al. Therapeutic peptides: Current applications and future directions. *Signal Transduct. Target Ther.* **7**(1), 48 (2022).
- Chiba, T. et al. Calcitonin gene-related peptide receptor antagonist human CGRP-(8–37). *Am. J. Physiol.* **256**(2 Pt 1), E331–E335 (1989).
- Kurtzhals, P. et al. Albumin binding of insulins acylated with fatty acids: characterization of the ligand-protein interaction and correlation between binding affinity and timing of the insulin effect in vivo. *Biochem. J.* **312**(Pt 3), 725–31 (1995).
- Lau, J. et al. Discovery of the once-weekly glucagon-like peptide-1 (GLP-1) analogue semaglutide. *J. Med. Chem.* **58**(18), 7370–7380 (2015).
- Ostergaard, S. et al. The effect of fatty diacid acylation of human PYY(3–36) on Y(2) receptor potency and half-life in minipigs. *Sci. Rep.* **11**(1), 21179 (2021).
- Sleep, D., Cameron, J. & Evans, L. R. Albumin as a versatile platform for drug half-life extension. *Biochim. Biophys. Acta* **1830**(12), 5526–5534 (2013).
- Zhang, L. & Bulaj, G. Converting peptides into drug leads by lipidation. *Curr. Med. Chem.* **19**(11), 1602–1618 (2012).
- Jonassen, I. et al. Design of the novel protraction mechanism of insulin degludec, an ultra-long-acting basal insulin. *Pharm. Res.* **29**(8), 2104–2114 (2012).

32. Santoprete, A. et al. DPP-IV-resistant, long-acting oxyntomodulin derivatives. *J. Pept. Sci.* **17**(4), 270–280 (2011).
33. Nielsen, J. C. et al. Machine-learning-guided peptide drug discovery: Development of GLP-1 receptor agonists with improved drug properties. *J. Med. Chem.* **67**, 11814–11826 (2024).
34. D'Santos, C. S. et al. Stimulation of adenylate cyclase by amylin in CHO-K1 cells. *Mol. Pharmacol.* **41**(5), 894–899 (1992).
35. Arunlakshana, O. & Schild, H. O. Some quantitative uses of drug antagonists. 1958. *Br. J. Pharmacol.* **120**(4 Suppl), 151–61 (1997).
36. Schild, H. O. pA, a new scale for the measurement of drug antagonism. 1947. *Br. J. Pharmacol.* **120**(4 Suppl), 29–46 (1997).
37. Lundberg, S.M.a.L., Su-In, A *Unified Approach to Interpreting Model Predictions.* (2017).
38. Hoare, S. R. Mechanisms of peptide and nonpeptide ligand binding to Class B G-protein-coupled receptors. *Drug Discov. Today* **10**(6), 417–427 (2005).
39. Madsen, K. et al. Structure-activity and protraction relationship of long-acting glucagon-like peptide-1 derivatives: Importance of fatty acid length, polarity, and bulkiness. *J. Med. Chem.* **50**(24), 6126–6132 (2007).
40. Knudsen, L. B. Glucagon-like peptide-1: The basis of a new class of treatment for type 2 diabetes. *J. Med. Chem.* **47**(17), 4128–4134 (2004).
41. Fletcher, M. M. et al. AM833 is a novel agonist of calcitonin family G protein-coupled receptors: Pharmacological comparison with six selective and nonselective agonists. *J. Pharmacol. Exp. Ther.* **377**(3), 417–440 (2021).
42. Kim, Y. G. et al. Peptidomics approach to elucidate the proteolytic regulation of bioactive peptides. *Proc. Natl. Acad. Sci. U. S. A.* **109**(22), 8523–8527 (2012).
43. Mimeault, M. et al. Comparative affinities and antagonistic potencies of various human calcitonin gene-related peptide fragments on calcitonin gene-related peptide receptors in brain and periphery. *J. Pharmacol. Exp. Ther.* **258**(3), 1084–1090 (1991).
44. Hay, D. L. et al. A comparison of the actions of BIBN4096BS and CGRP(8–37) on CGRP and adrenomedullin receptors expressed on SK-N-MC, L6, Col 29 and Rat 2 cells. *Br. J. Pharmacol.* **137**(1), 80–86 (2002).
45. Lang, M. et al. Identification of the key residue of calcitonin gene related peptide (CGRP) 27–37 to obtain antagonists with picomolar affinity at the CGRP receptor. *J. Med. Chem.* **49**(2), 616–624 (2006).
46. Watkins, H. A. et al. Structure-activity relationships for alpha-calcitonin gene-related peptide. *Br. J. Pharmacol.* **170**(7), 1308–1322 (2013).
47. Booe, J. M. et al. Probing the mechanism of receptor activity-modifying protein modulation of GPCR ligand selectivity through rational design of potent adrenomedullin and calcitonin gene-related peptide antagonists. *Mol. Pharmacol.* **93**(4), 355–367 (2018).
48. ter Haar, E. et al. Crystal structure of the ectodomain complex of the CGRP receptor, a class-B GPCR, reveals the site of drug antagonism. *Structure* **18**(9), 1083–1093 (2010).
49. Liang, Y. L. et al. Cryo-EM structure of the active, G(s)-protein complexed, human CGRP receptor. *Nature* **561**(7724), 492–497 (2018).
50. Hoare, S. R. J. The problems of applying classical pharmacology analysis to modern in vitro drug discovery assays: Slow binding kinetics and high target concentration. *SLAS Discov.* **26**(7), 835–850 (2021).
51. Charlton, S. J. & Vauquelin, G. Elusive equilibrium: the challenge of interpreting receptor pharmacology using calcium assays. *Br. J. Pharmacol.* **161**(6), 1250–1265 (2010).
52. Christensen, S. L. et al. CGRP-dependent signalling pathways involved in mouse models of GTN- cilostazol- and levromakalim-induced migraine. *Cephalalgia* **41**(14), 1413–1426 (2021).
53. Gangula, P. R. et al. Mesenteric arterial relaxation to calcitonin gene-related peptide is increased during pregnancy and by sex steroid hormones. *Biol. Reprod.* **71**(5), 1739–1745 (2004).
54. Edvinsson, L. et al. Differential localization and characterization of functional calcitonin gene-related peptide receptors in human subcutaneous arteries. *Acta Physiol. (Oxf.)* **210**(4), 811–822 (2014).
55. Sheykhzade, M. et al. Binding and functional pharmacological characteristics of gepant-type antagonists in rat brain and mesenteric arteries. *Vascul. Pharmacol.* **90**, 36–43 (2017).
56. de Vries, T. et al. Blocking the CGRP Receptor: Differences across Human Vascular Beds. *Pharmaceuticals (Basel)* **16**(8), 1075 (2023).
57. McNeish, A. J. et al. Endosomal proteolysis regulates calcitonin gene-related peptide responses in mesenteric arteries. *Br. J. Pharmacol.* **167**(8), 1679–1690 (2012).

Author contributions

L.E., B.B.G., M.L., J.C.N., D.M.J., F.A., K.A.H., and J.B.K. conceived and designed the experiments. Peptide synthesis and associated chemistry was performed by M.K. and F.A. Bioanalysis was performed by U.L. and bioinformatics were done by J.C.N. Data analysis and interpretation was done L.E., B.B.G., H.H.H., M.L., U.L., J.C.N., F.A. and J.B.K., M.D. and K.A.H. The manuscript was written by J.B.K., K.A.H., M.D., and H.H.H. All authors approved of the final manuscript.

Funding

This study was supported by a PhD grant (M.D. and J.B.K.) from Innovation Fund Denmark (grant no. 2040-00060B). L.E., M.L., J.C.N., D.M.J., H.H.H., M.K., U.L., M.D. and J.B.K. are employed by Gubra. B.B.G. and F.A. were previously employed by Gubra and are currently employed by Novo Nordisk. K.A.H. was supported by a Lundbeck foundation Fellowship (R345-2020-1977).

Declarations

Competing interests

J.B.K., M.L., D.M.J. and H.H.H. owns stocks at Gubra. B.B.G., F.A., U.L., J.C.N., L.E. M.D., K.A.H. and M.K. declare no competing interests.

Additional information

Correspondence and requests for materials should be addressed to J.B.K. or M.D.

Reprints and permissions information is available at www.nature.com/reprints.

Publisher's note Springer Nature remains neutral with regard to jurisdictional claims in published maps and institutional affiliations.

Open Access This article is licensed under a Creative Commons Attribution-NonCommercial-NoDerivatives 4.0 International License, which permits any non-commercial use, sharing, distribution and reproduction in any medium or format, as long as you give appropriate credit to the original author(s) and the source, provide a link to the Creative Commons licence, and indicate if you modified the licensed material. You do not have permission under this licence to share adapted material derived from this article or parts of it. The images or other third party material in this article are included in the article's Creative Commons licence, unless indicated otherwise in a credit line to the material. If material is not included in the article's Creative Commons licence and your intended use is not permitted by statutory regulation or exceeds the permitted use, you will need to obtain permission directly from the copyright holder. To view a copy of this licence, visit <http://creativecommons.org/licenses/by-nc-nd/4.0/>.

© The Author(s) 2024